

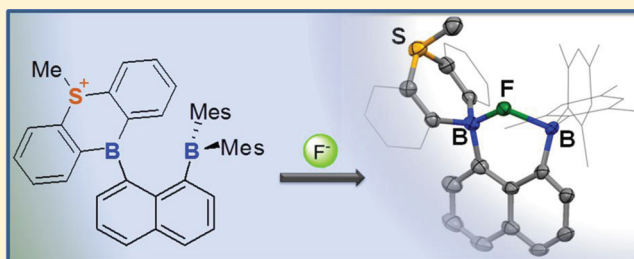
On the Synergy of Coulombic and Chelate Effects in Bidentate Diboranes: Synthesis and Anion Binding Properties of a Cationic 1,8-Diborylnaphthalene

Haiyan Zhao and François P. Gabbaï*

Department of Chemistry, Texas A&M University, College Station, Texas 77843-3255, United States

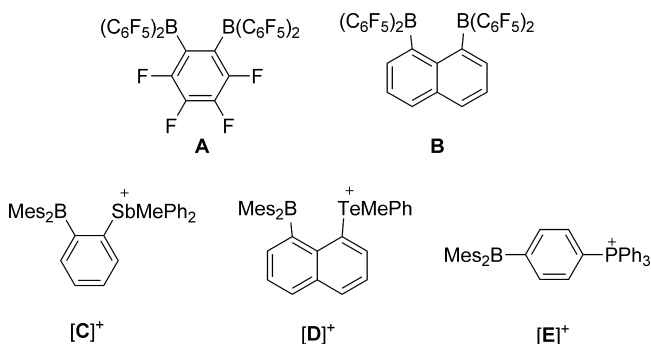
Supporting Information

ABSTRACT: As part of our investigation in the chemistry of bidentate Lewis acids for anion complexation, we have carried out the reaction of 1-(dimesitylboryl)-8-(1'-bora-9'-thianthryl)naphthalene (**1**) with methyltriflate. This reaction proceeds via alkylation of the sulfur atom to afford a bidentate diborane (**[2]⁺**) decorated by a peripheral sulfonium unit. This new diborane, which has been isolated as the triflate salt, reacts with both fluoride and azide anions to form the corresponding anion chelate complexes **2-μ₂-F** and **2-μ₂-N₃**, respectively. Titration experiments carried out in chloroform indicate that the fluoride binding constant of **[2]⁺** exceeds that of **1** by at least 4 orders of magnitude. These results, which are supported by spectroscopic, structural, and computational data, show that chelate and Coulombic effects are additive and can be combined to boost the anion affinity of bidentate Lewis acids.



INTRODUCTION

The chemistry of boron-based bidentate Lewis acids¹ is an area of active investigation with application in the domains of anion complexation,² organometallic catalysis,³ and small-molecule activation.⁴ Since the properties of these bidentate Lewis acids can be influenced by the respective positions and electronic features of the binding sites, a great deal of attention has been dedicated to the synthesis of compounds with juxtaposed electron-poor boron functionalities.^{3a,4a} Prototypical examples of such compounds include the fluorinated diboranes **A** and **B**, which have both been shown to chelate small anions.^{3a,4a}



In a variant of this approach, several groups, including ours, have become interested in boron-based bidentate Lewis acids that bear a cationic group in proximity to the boron atom.^{3d,5} Examples of such compounds include **[C]⁺** and **[D]⁺**, which have been investigated for the complexation of fluoride anions.^{5h,i} For these compounds, the coordination of the anion is supported by the formation of a B–F→Sb (for **[C]⁺**)

or B–F→Te (for **[D]⁺**) motif, whose formation illustrates the Lewis acidic behavior of the heavy onium moiety. The stability of the resulting complexes also benefits from strong Coulombic effects, which prevent dissociation of the anion from the cationic host. The favorable influence of these Coulombic effects has also been demonstrated in the case of triarylboranes decorated by peripheral cationic moieties such as the phosphonium borane **[E]⁺**, which, unlike neutral boranes, captures F[−] in aqueous solution.^{5j}

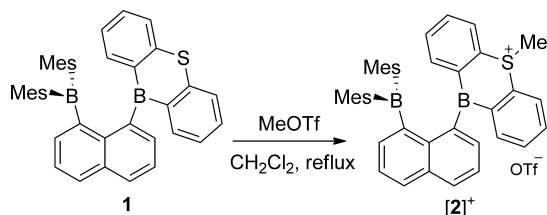
Building on these earlier achievements, we have now decided to target bidentate diboranes that incorporate a peripheral cationic functionality. From a simple conceptual viewpoint, we anticipate that the anion affinity of such system would benefit from (i) the chelate effect provided by the chelating diborane moiety; (ii) the Coulombic effect imparted by the presence of a peripheral cationic group.

RESULTS AND DISCUSSION

Synthesis and Characterization of the Cationic Bidentate Lewis Acid. Inspired by Katz's seminal contribution on the anion affinity of 1,8-dimethylborylnaphthalene,^{1b,6} our group has investigated the synthesis of numerous naphthalene-based diboranes⁷ including **1** (Scheme 1),⁸ whose fluoride binding constants exceed that of monofunctional analogues by at least 3 or 4 orders of magnitude. With the synthesis of a cationic bidentate borane as an objective, it occurred to us that the sulfur atom of the thiaborin⁹ moiety

Received: December 8, 2011

Published: March 9, 2012

Scheme 1. Synthesis of the Sulfonium Diborane of [2]⁺

could possibly be alkylated. With this in mind, **1** was allowed to react with MeOTf in refluxing dichloromethane to afford [2]OTf as a moisture-sensitive compound (Scheme 1). This salt has been characterized by NMR spectroscopy, UV–vis spectroscopy, and single-crystal X-ray diffraction. The ¹H NMR spectrum of this compound shows a singlet at 3.60 ppm corresponding to the methyl group of the sulfonium ion. In addition, six distinct methyl groups are observed for the mesityl substituents, indicating that the structure of [2]⁺ is sterically congested. Although the S-alkylation of thiaborins has, to our knowledge, never been reported, we note that related reactions are known for phosphaborins, which can be easily converted into the corresponding phosphonium species.¹⁰

The crystal structure of [2]OTf shows that (1) both boron centers B(1) and B(2) adopt a trigonal-planar coordination geometry, as indicated by the sum of the C_{aryl}–B–C_{aryl} angles ($\sum \angle C-B(1)-C = 356.02^\circ$, $\sum \angle C-B(2)-C = 359.55^\circ$); (2) the distance separating the two boron atoms (3.276(3) Å) is almost identical to that of the neutral precursor **1** (3.279(4) Å); and (3) the sulfur-bound methyl group points outward from the diboron pocket (Figure 1). The UV–vis spectrum of

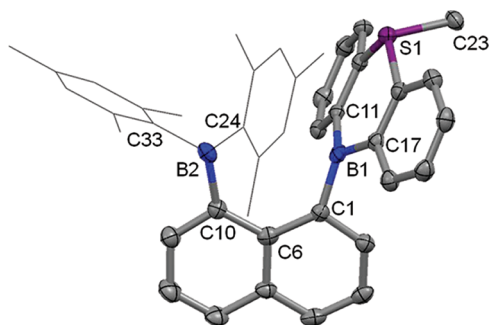


Figure 1. ORTEP drawing of [2]⁺ with thermal ellipsoid plots (50% probability). For clarity, the hydrogen atoms and triflate anion are omitted, and the mesityl substituents are represented by a thin line. Selected bond lengths (Å) and angles (deg): S(1)–C(23) 1.796(2), C(1)–B(1) 1.568(3), C(17)–B(1) 1.569(3), C(11)–B(1) 1.564(3), C(24)–B(2) 1.576(3), C(33)–B(2) 1.578(3), C(10)–B(2) 1.567(3); C(11)–B(1)–C(1) 117.23(18), C(11)–B(1)–C(17) 117.97(18), C(1)–B(1)–C(17) 120.82(18), C(10)–B(2)–C(24) 124.41(18), C(10)–B(2)–C(33) 116.85(17), C(24)–B(2)–C(33) 118.29(17), C(6)–C(10)–B(2) 128.27(17), C(6)–C(1)–B(1) 131.89(17).

[2]OTf in CHCl₃ exhibits a band centered at $\lambda_{\max} = 349$ nm.¹¹ This band, whose position is close to that observed for **1** ($\lambda_{\max} = 363$ nm in THF),^{8a} originates from the trigonal-planar boron-centered chromophores, thus implying that the triflate counteranion does not associate with [2]⁺ in solution. To confirm this photophysical assignment, the structure of [2]⁺ has been computationally optimized using DFT methods (functional: B3LYP; mixed basis set: B: 6-31+G(d'); S: 6-31+G(d); C, H: 6-31G). The optimized geometry, which is close to that

determined experimentally, was subjected to a time-dependent DFT calculation using the PCM solvation model with chloroform as a solvent. The LUMO of [2]⁺ is localized on the cationic and thus inherently electron-deficient sulfonium boryl moiety, with a dominating contribution from the p_z orbital of the boron atom. The LUMO+1 is centered on the other boryl moiety, again with a large contribution from the p_z orbital of the boron atom. These orbital characteristics contrast with those of the neutral precursor **1**, for which the LUMO shows an almost equal contribution from both boron p_z orbitals (Figure 2).^{8,12} These differences illustrate the asymmetry induced by the cationic sulfonium moiety, making one side of the molecule distinctly more electron-deficient than the other one. TD-DFT calculations indicate that both the LUMO and LUMO+1 of [2]⁺ are the main accepting orbitals of the electronic transitions that contribute to the low-energy band observed at $\lambda_{\max} = 349$ nm. We have also compared the electrochemical properties of **1** and [2]⁺. Unlike the cyclic voltammogram of **1**, which shows two reversible reduction waves at $E_{1/2} = -2.20$ V and -2.57 V (vs Fc/Fc⁺),^{8b} [2]⁺ displays an irreversible wave only at $E_{\text{red}} = -1.66$ V (vs Fc/Fc⁺) in THF. The potential of this wave, which is much more positive than that of **1**, indicates that [2]⁺ is substantially more electrophilic than **1**. Its irreversibility also suggests that the resulting neutral radical is unstable.

Fluoride Anion Complexation. The cationic borane [2]⁺ quickly reacts with [*n*Bu₄N][Ph₃SiF₂] in CDCl₃ to afford the corresponding fluoride complex 2- μ_2 -F, as confirmed by NMR spectroscopy. Synthesis of this fluoride adduct can also be carried out in CH₂Cl₂ by reaction of [2]OTf with [(Me₂N)₃S]-[Me₃SiF₂]. Adduct 2- μ_2 -F, which is air and moisture stable, has been fully characterized. The ¹¹B NMR resonances at -0.4 and 4.4 ppm are consistent with the presence of two four-coordinate boron centers.^{8a} The ¹H NMR resonance of the sulfur-bound methyl group appears at 3.28 ppm, upfield from that of [2]⁺ at 3.60 ppm. The ¹⁹F NMR signal at -174.4 ppm is comparable to the chemical shift observed in other fluoride chelate complexes^{3a} including [1- μ_2 -F]⁻ (-188.7 ppm).^{8a} The structure of 2- μ_2 -F has also been determined by single-crystal X-ray diffraction (Figure 3). In contrast with the relatively symmetrical B–F–B bridge of [1- μ_2 -F]⁻ (B–F bond lengths = 1.585(5) and 1.633(5) Å),^{8a} the structure of 2- μ_2 -F shows that the fluorine atom forms a short bond with B(1) (1.539(4) Å) and a long one with B(2) (1.822(4) Å). This unsymmetrical coordination is logically reflected by a notable difference in the extent of pyramidalization observed for each boron center ($\sum(\angle C-B(1)-C) = 334.6^\circ$ and $\sum(\angle C-B(2)-C) = 350.6^\circ$). The asymmetry of the B–F–B bridge in 2- μ_2 -F can be correlated to the presence of a sulfonium moiety, which enhances the Lewis acidity of the adjacent B(1) atom. This conclusion is in agreement with the computational studies of [2]⁺ that show that the p_z orbital of the B(1) boron atom contributes to the LUMO, while that of the B(2) atom contributes to the LUMO+1. It is also interesting to note that the sulfur-bound methyl group is oriented inward. This surprising orientation places the C(41) atom at 3.452 Å from the fluorine atom, which is above the range that one would expect if a C_{Me}–H...F interaction was present.

The structure of 2- μ_2 -F has been computationally optimized using DFT methods (functional: B3LYP; mixed basis set: B: 6-31+G(d'); S: 6-31+G(d); C, H: 6-31G). Interestingly, the optimized structure shows a large deviation from that observed experimentally (Figure 4). The largest deviation is observed in

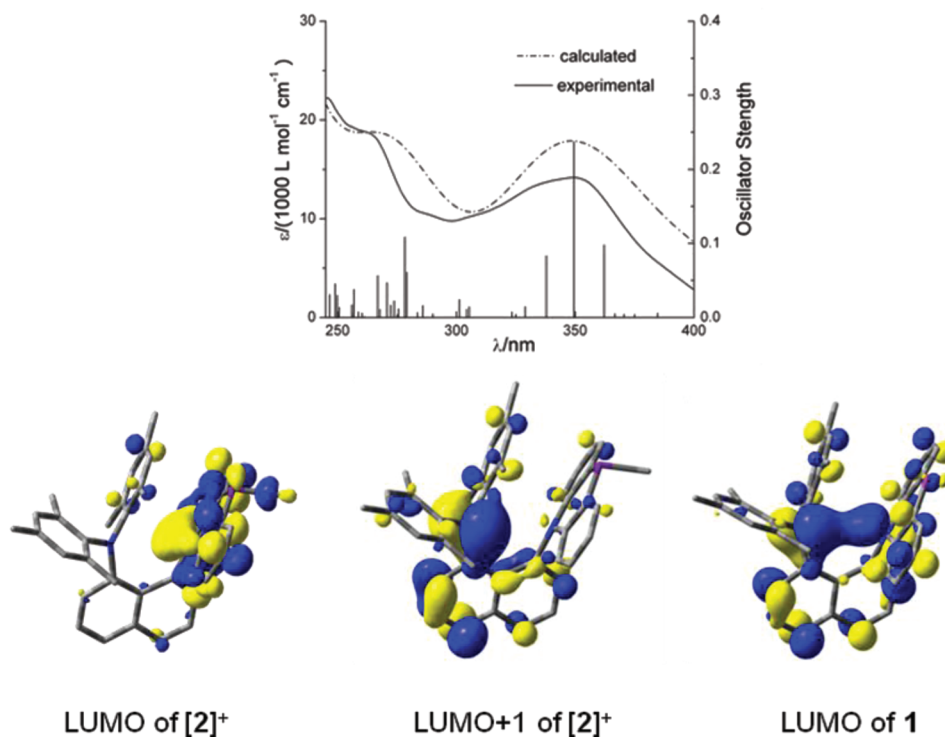
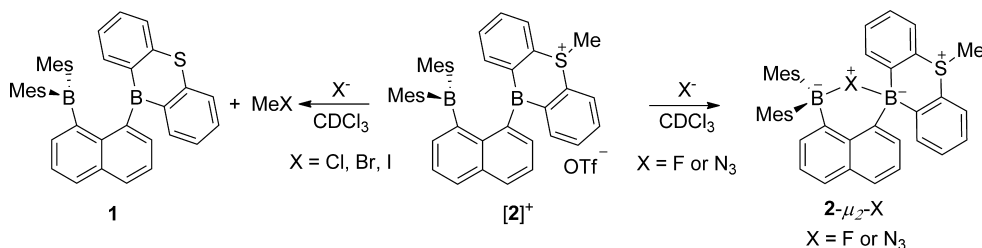


Figure 2. Top: Experimental (chloroform) and calculated UV-vis spectra for $[2]^+$. Bottom: Views of LUMO and LUMO+1 of $[2]^+$ and LUMO of **1** (isovalue = 0.035).

Scheme 2. Reactions of $[2]^+$ with Different Anions in Chloroform^a



^aAll charges appearing in the scheme are formal charges.

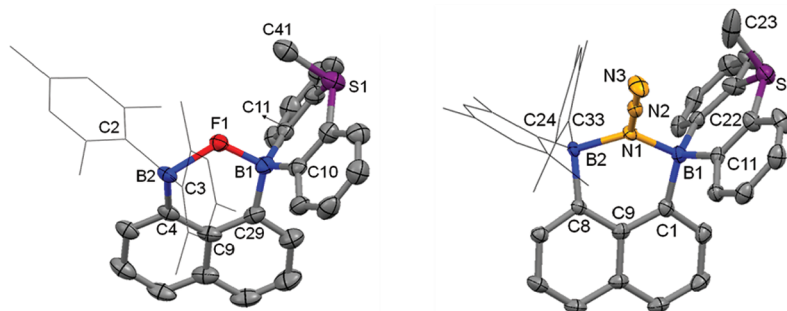


Figure 3. ORTEP drawings of $2-\mu_2\text{-F}$ and $2-\mu_2\text{-N}_3$ with thermal ellipsoid plots (50% probability). For clarity, the hydrogen atoms are omitted and the mesityl substituents are represented by a thin line. Selected bond lengths (Å) and angles (deg) for $2-\mu_2\text{-F}$: F(1)–B(1) 1.540(5), F(1)–B(2) 1.822(4), C(2)–B(2) 1.608(6), C(3)–B(2) 1.626(5), C(4)–B(2) 1.599(6), C(10)–B(1) 1.622(6), C(11)–B(1) 1.631(6), C(29)–B(1) 1.604(6), S(1)–C(41) 1.760(4); B1–F1–B2 124.1(2), C(29)–B(1)–C(10) 112.8(3), C(29)–B(1)–C(11) 110.3(3), C(10)–B(1)–C(11) 111.5(3), C(9)–C(29)–B(1) 125.5(3), C(4)–B(2)–C(2) 112.3(3), C(4)–B(2)–C(3) 120.3(3), C(2)–B(2)–C(3) 118.0(3), C(9)–C(4)–B(2) 125.2(3). Selected bond lengths (Å) and angles (deg) for $2-\mu_2\text{-N}_3$: N(1)–N(2) 1.243(5), N(1)–B(1) 1.643(6), N(1)–B(2) 1.704(6), N(2)–N(3) 1.136(5), C(1)–B(1) 1.621(7), C(11)–B(1) 1.637(6), C(22)–B(1) 1.626(7), C(24)–B(2) 1.653(6), C(8)–B(2) 1.622(6), C(33)–B(2) 1.652(6), S(1)–C(23) 1.714(7); B(1)–N(1)–B(2) 124.3(3), C(9)–C(1)–B(1) 125.8(4), C(9)–C(8)–B(2) 124.4(4), C(1)–B(1)–C(11) 111.0(4), C(1)–B(1)–C(22) 111.8(4), C(11)–B(1)–C(22) 112.1(4), C(8)–B(2)–C(33) 115.9(4), C(8)–B(2)–C(24) 108.7(3), C(33)–B(2)–C(24) 119.5(4).

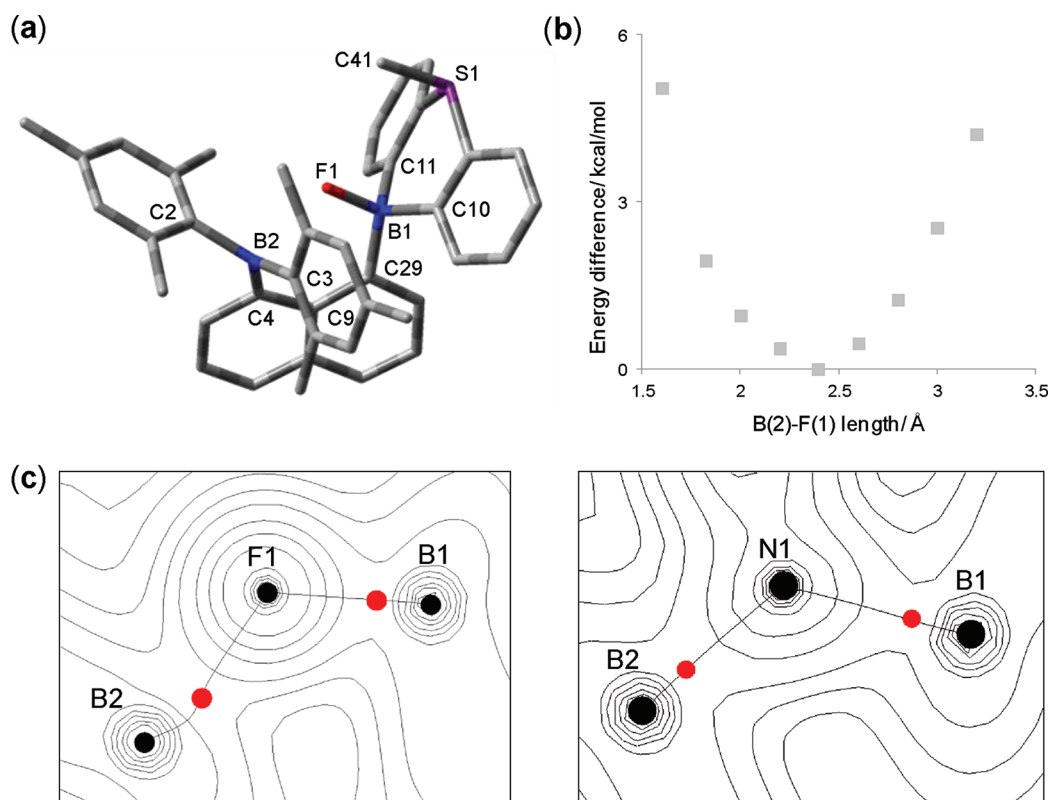


Figure 4. (a) Optimized structure of $2-\mu_2\text{-F}$. Calculated bond lengths (Å) and angles (deg) for $2-\mu_2\text{-F}$: F(1)–B(1) 1.486, F(1)–B(2) 2.393, C(2)–B(2) 1.604, C(3)–B(2) 1.601, C(4)–B(2) 1.589, C(10)–B(1) 1.648, C(11)–B(1) 1.658, C(29)–B(1) 1.625, S(1)–C(41) 1.836; B1–F1–B2 116.9, C(29)–B(1)–C(10) 113.0, C(29)–B(1)–C(11) 109.6, C(10)–B(1)–C(11) 110.2, C(9)–C(29)–B(1) 127.2, C(4)–B(2)–C(2) 116.2, C(4)–B(2)–C(3) 122.0, C(2)–B(2)–C(3) 119.3, C(9)–C(4)–B(2) 129.0. (b) Energy changes based on different B(2)–F(1) lengths in the optimization calculations of $2-\mu_2\text{-F}$. (c) AIM electron density maps with relevant bond paths and bond critical points of the B(1)–F(1)–B(2) bond in $2-\mu_2\text{-F}$ (left) and the B(1)–N(1)–B(2) bond in $2-\mu_2\text{-N}_3$ (right).

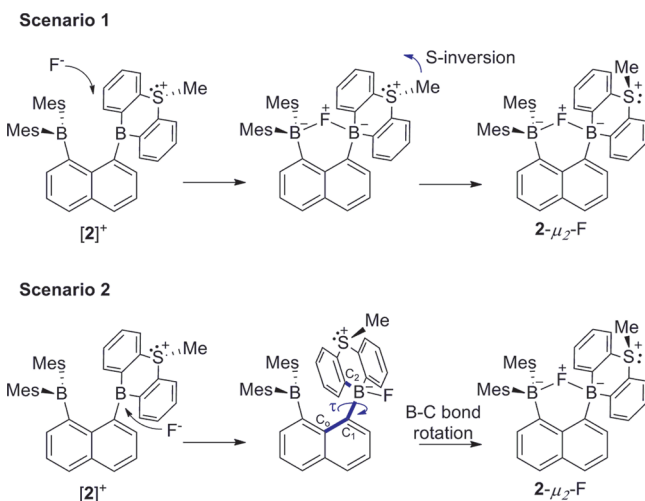
the B(2)–F(1) bond, which converges to a value of 2.393 Å as opposed to 1.822(4) Å in the crystal structure. To elucidate the origin of this difference, we decided to study how variations in the B(2)–F(1) bond length affect the total energy of the structure. To this end, the structure of $2-\mu_2\text{-F}$ has been optimized with the B(2)–F(1) constrained at 1.600, 1.822, 2.000, 2.200, 2.400, 2.600, 2.800, 3.000, and 3.200 Å. As it can be seen from Figure 4, the total energy of the molecule varies by only 1.95 kcal/mol in the 1.822 < B(2)–F(1) < 2.800 Å range. This shallow energy well indicates that the B(2)–F(1) bond length has a limited effect on the total energy of the molecule, the structure of which can therefore be influenced by subtle solvation or crystal packing effects.

A geometry optimization carried out by constraining the B(2)–F(1) bond length to its experimental value (B(2)–F(1) = 1.822 Å) afforded a structure that lies only 1.95 kcal/mol above the computed minimum with a B(1)–F(1) bond length of 1.555 Å (Figure 4). The latter is in good agreement with the B(1)–F(1) bond length of 1.540(5) Å determined by X-ray diffraction (Figure 3). An atom in molecules (AIM) calculation¹³ carried out at this constrained geometry identifies a bond path for both the B(1)–F(1) and the B(2)–F(2) linkages (Figure 4). The electron density $\rho(r)$ of 0.100 e bohr⁻³ at the bond critical point (BCP) of the B(1)–F(1) bond is significantly larger than that of the B(2)–F(1) bond (0.053 e bohr⁻³), in agreement with the observed asymmetry of the B–F–B bridge. By contrast, AIM calculations carried out at the optimized geometry of the $[\text{I}-\mu_2\text{-F}]^-$ indicate a much more symmetrical B–F–B bridge, with similar electron density at the

BCP of the B(1)–F(1) bond ($\rho(r) = 0.074 \text{ e bohr}^{-3}$) and B(2)–F(1) bond ($\rho(r) = 0.077 \text{ e bohr}^{-3}$).

Another point that we decided to address computationally is the change observed in the orientation of the sulfur-bound methyl group, which switches from outward in $[\text{2}]^+$ to inward in 2-F. A priori, this change could occur by inversion of the sulfonium atom after fluoride complexation (scenario 1, Scheme 3). Alternatively, a fluoride anion could first bind externally to the boron atom of the thiaborinium fragment, followed by rotation of the resulting fluoroborate moiety about the B–C₁ bond connecting the thiaborinium to the naphthalene backbone (scenario 2, Scheme 3). To test the first scenario, we carried out a transition-state calculation (functional: B3LYP; mixed basis set: B: 6-31+G(d'); S: 6-31+G(d); C, H: 6-31G), which indicates that the energy barrier to inversion of the sulfonium unit is equal to 27.11 kcal/mol. For the second scenario we scanned the energy of the complex as a function of the C₀–C₁–B–C₂ torsional angle (denoted as τ , Scheme 3) between the values of 101.3° found by optimization of the exo/noncholate complex 2-F and –103.6° found by the unconstrained optimization of the chelate complex $2-\mu_2\text{-F}$. To this end, the structure of the molecule was optimized with the angle τ constrained to 40°, 20°, 10°, 0°, –10°, –20°, and –40°. The energies of the resulting structures, which are plotted in Figure 5, show that this rotation is a relatively low-energy pathway, the barrier of which does not exceed 14 kcal/mol. This barrier to rotation is almost 50% lower than the barrier determined for the inversion of the sulfonium unit. Accordingly, we propose that the change observed in the

Scheme 3. The Two Different Scenarios Envisaged for the Switching of the Methyl Group from Outward in $[2]^+$ to Inward in $2-\mu_2\text{-F}^a$



^aAll charges appearing in the scheme are formal charges.

orientation of the sulfur-bound methyl group upon conversion of $[2]^+$ into $2-\mu_2\text{-F}$ occurs via scenario 2. These computational results also indicate that rotations of the groups at the *peri*-positions of these naphthalene systems are not energetically prohibited despite the large steric crowding affecting these compounds.

To further understand the influence of the cationic sulfonium moiety in $[2]^+$, we decided to measure the fluoride binding constant of $[2]^+$ and compare it to that of **1**. Since we have previously shown that the binding constant of neutral **1** exceeds the range measurable by a direct titration with tetrabutylammonium fluoride ($n\text{Bu}_4\text{NF}$),^{8a} we decided to employ the commercially available tetrabutylammonium difluorotriphenylsilicate $[n\text{Bu}_4\text{N}][\text{Ph}_3\text{SiF}_2]$ as fluoride source and determine the relative binding constant $K_{\text{rel}}(\text{borane}) = K(\text{borane})/K(\text{Ph}_3\text{SiF})$,

where $K(\text{borane})$ is the absolute fluoride binding constant of the borane under study and $K(\text{Ph}_3\text{SiF})$ is the absolute fluoride binding constant of Ph_3SiF (see Experimental Section for details of the derivation). $K_{\text{rel}}(\mathbf{1})$ could be derived from the integrated ^1H NMR and ^{19}F NMR spectra of CDCl_3 solutions containing **1** and $[n\text{Bu}_4\text{N}][\text{Ph}_3\text{SiF}_2]$ in different molar ratios, affording $K_{\text{rel}}(\mathbf{1}) = 5.4 (\pm 1)$ (see SI for details of the experiments). Analogous NMR experiments carried out with $[2]^+$ indicated the quantitative formation of $2-\mu_2\text{-F}$. For this reason, we decided to resort to UV-vis spectroscopy, which is more appropriate to study large binding constants. However, addition of $[n\text{Bu}_4\text{N}][\text{Ph}_3\text{SiF}_2]$ to a dilute chloroform solution of $[2]^+$ (6.7×10^{-5} M in CHCl_3) resulted in the stoichiometric quenching of the absorbance of the boron-centered chromophore at 349 nm, in agreement with the quantitative formation of the fluoride complex (Figure 6). These observations indicate that the relative fluoride binding constant of $[2]^+$ ($K_{\text{rel}}([2]^+)$) exceeds the value of 10^5 and is thus at least 4 orders of magnitude greater than that of **1**. The drastic difference observed in the fluoride binding properties of **1** and $[2]^+$ underscores the higher fluoride affinity of $[2]^+$, which can be assigned to its cationic nature. Although $2-\mu_2\text{-F}$ is very stable, it slowly reacts with $\text{B}(\text{C}_6\text{F}_5)_3$ to afford $[2][\text{FB}(\text{C}_6\text{F}_5)_3]$, thus indicating that fluoride binding by $[2]^+$ is reversible. A similar reaction was observed for $[1-\mu_2\text{-F}]^-$, which also releases fluoride to $\text{B}(\text{C}_6\text{F}_5)_3$.^{8a}

We also decided to compare the fluoride anion affinity of $[2]^+$ to that of another cationic borane. For the purpose of this study, we selected the phosphonium borane $[3]^+$, which was previously shown to react with fluoride to afford 3-F .^{5b} Interestingly, mixing equimolar amounts of $[2]^+$ and 3-F in CDCl_3 at ambient temperature leads to the quantitative formation of $[3]^+$ and $2-\mu_2\text{-F}$ (Scheme 4). Fluoride ion transfer from 3-F to $[2]^+$ is confirmed by ^1H , ^{19}F , and ^{31}P NMR spectroscopy. Specifically, the ^{31}P NMR spectrum shows full conversion of 3-F (28.3 ppm) into $[3]^+$ (23.9 ppm). Accordingly, the ^{19}F NMR spectrum indicates formation of $2-\mu_2\text{-F}$, the resonance of which appears at -174.4 ppm. Related changes are also observed in the ^1H NMR spectrum, where the

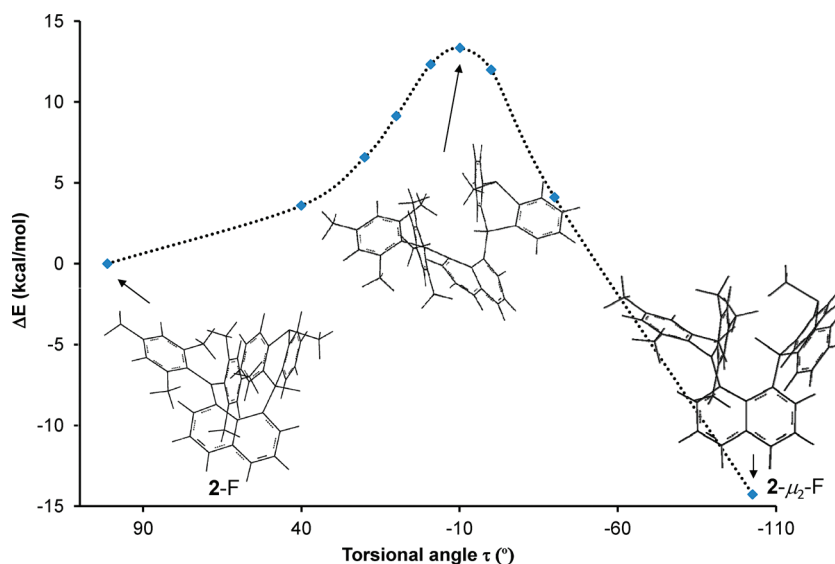


Figure 5. Relative energy of 2-F as a function of the torsional angle τ as defined in Scheme 3. The first point of the graph (left) corresponds to the exo/noncholate complex 2-F , the energy of which is taken as the reference ($\tau = 101.3^\circ$). The last point of the graph (right) corresponds to $2-\mu_2\text{-F}$ ($\tau = 103.6^\circ$). The structure shown in the middle is that obtained for $\tau = -10^\circ$. The fitted line is arbitrary and does not accurately map the energy profile of the process.

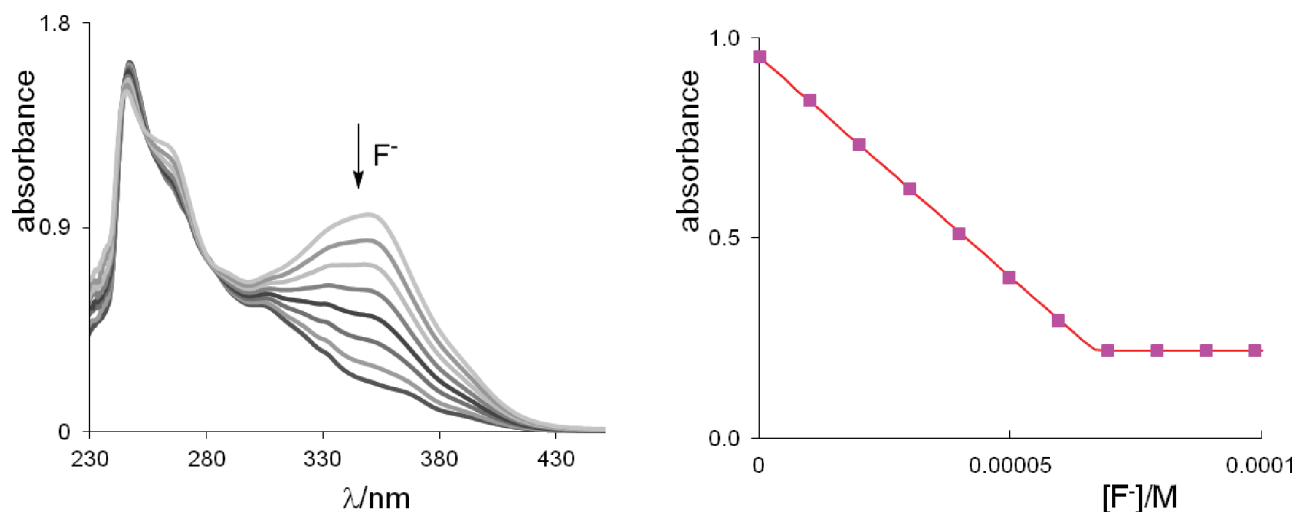
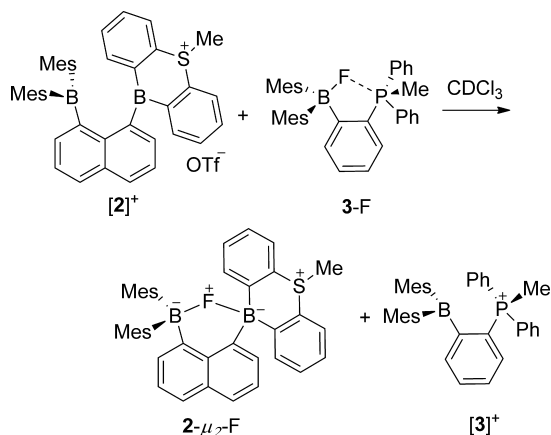


Figure 6. Left: Absorbance changes upon addition of $[n\text{Bu}_4\text{N}][\text{Ph}_3\text{SiF}_2]$ to a CHCl_3 solution of $[2]^+$ (0.067 mM). Right: Binding isotherm monitored at $\lambda = 349$ nm ($K_{\text{rel}}([2]^+) \geq 10^5$, $\epsilon = 10\,040$ for $[2]\text{OTf}$, $\epsilon = 3270$ for $2\text{-}\mu_2\text{-F}$).

Scheme 4. Competition Reaction of $[2]^+$ with 3-F in CDCl_3 ^a



^aAll charges appearing in the scheme are formal charges.

P- or *S*-bound methyl signals of $[2]^+$ (3.60 ppm) and 3-F (3.12 ppm) disappear to give rise to those of $2\text{-}\mu_2\text{-F}$ (3.28 ppm) and $[3]^+$ (2.67 ppm). This reaction indicates that $[2]^+$ is one of the most Lewis acidic cationic boranes ever investigated in our

group. Presumably the cumulative Coulombic and chelate effects occurring with this compound are responsible for this enhanced fluoride affinity.

Reaction with Other Anions. To conclude this study, we decided to probe the reactivity of $[2]^+$ toward other anions. Interestingly, addition of $n\text{Bu}_4\text{Cl}$, $n\text{Bu}_4\text{Br}$, or $n\text{Bu}_4\text{I}$ to a CDCl_3 solution of $[2]^+$ resulted in the formation of the neutral diborane **1**, indicating demethylation of the diarylmethylsulfonium (Scheme 2). Such demethylation reactions are not unprecedented and have been observed in related sulfonium borane species.^{3d,14} The reactivity of $[2]^+$ toward cyanide was also tested using $n\text{Bu}_4\text{CN}$ as a cyanide source. In this case, however, the reaction afforded a mixture of compounds that could not be unambiguously identified. A cleaner anion complexation reaction was observed with $n\text{Bu}_4\text{N}_3$ in CDCl_3 , leading to the corresponding azide complex $2\text{-}\mu_2\text{-N}_3$. Formation of the latter, which can be reverted by addition of $\text{B}(\text{C}_6\text{F}_5)_3$, could be monitored by UV-vis spectroscopy to afford a binding constant exceeding 10^7 M^{-1} (Figure 7).

The azide complex $2\text{-}\mu_2\text{-N}_3$, which could be isolated from the reaction of $[2]\text{OTf}$ with $n\text{Bu}_4\text{N}_3$ in dichloromethane, has been fully characterized. It features a broad ^{11}B NMR resonance

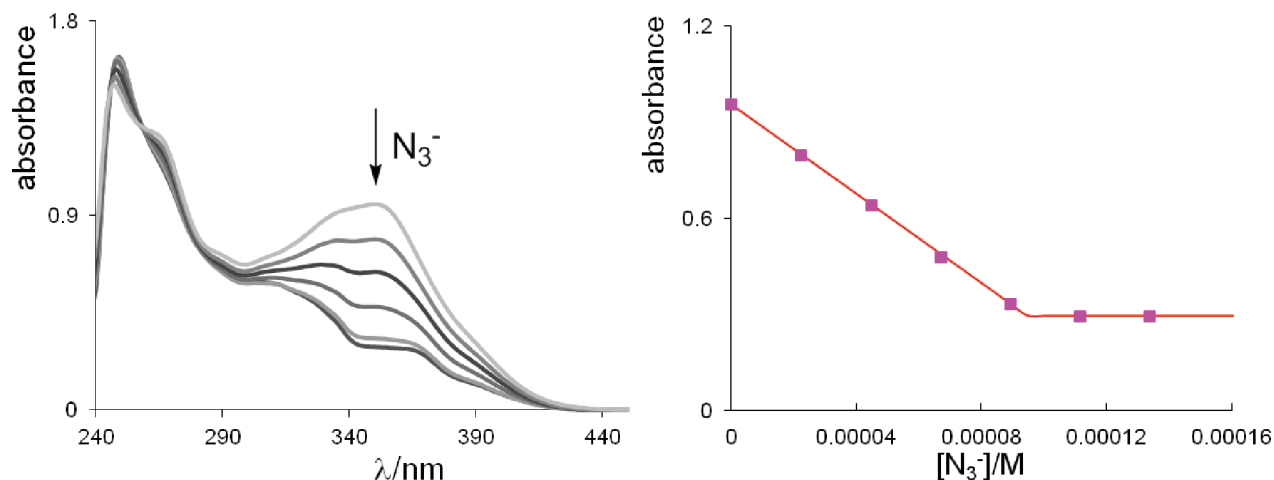


Figure 7. Left: Absorbance changes upon addition of $n\text{Bu}_4\text{N}_3$ to a CHCl_3 solution of $[2]^+$ (0.095 mM). Right: Binding isotherm monitored at $\lambda = 349$ nm ($K \geq 10^7$ M^{-1} , $\epsilon = 10\,040$ for $[2]\text{OTf}$, $\epsilon = 3100$ for $2\text{-}\mu_2\text{-N}_3$).

at -4.6 ppm, which, we speculate, corresponds to the overlapping signals of the two four-coordinate boron centers. In line with the coordination of an anion to the diborane, the resonance of the sulfur-bound methyl group at 3.26 ppm is close to that measured for $2-\mu_2\text{-F}$ (3.28 ppm). The crystal structure of $2-\mu_2\text{-N}_3$ confirms formation of a chelate complex, with the azide anion bridging the two boron centers in a $\mu-\eta^1$ fashion (Figure 3). While the structure of $2-\mu_2\text{-F}$ showed a rather unsymmetrical B–F–B bridge, the N(1)–B(1) (1.635 Å) and N(1)–B(2) (1.706 Å) bond lengths in $2-\mu_2\text{-N}_3$ indicate a rather symmetrical B–N–B bridge, which is consistent with the propensity of the azide anion to adopt a $\mu-\eta^1$ coordination mode. The DFT-optimized structure $2-\mu_2\text{-N}_3$ (functional: B3LYP; mixed basis set: B, N: 6-31+G(d); S: 6-31+G(d); C, H: 6-31G) features a B(1)–N(1) distance of 1.644 Å, which is very close to that experimentally observed. The calculated N(1)–B(2) distance of 1.832 Å is slightly elongated when compared to that experimentally observed, a phenomenon reminiscent of that observed in the computed structure of $2-\mu_2\text{-F}$. Presumably, small variation of this bond length has only a limited effect on the total energy of the molecule, making subtle solvation or crystal packing effects the main culprit for this small discrepancy. An AIM analysis carried out at the optimized geometry affords consistent results with BCP electron densities $\rho(r) = 0.108$ e bohr $^{-3}$ for N(1)–B(1) and $\rho(r) = 0.070$ e bohr $^{-3}$ for N(1)–B(2), again illustrating the increased acidity of the sulfonium-decorated boryl moiety (Figure 4).

CONCLUSION

As demonstrated by our earlier work on naphthalene-based diboranes,^{2a} the fluoride binding constants of neutral bidentate derivatives exceed those of their monofunctional analogues by 3 or 4 orders of magnitude. The results presented in this paper show that the fluoride anion affinity of such diboranes can be further enhanced by the simple introduction of a cationic moiety in the proximity of one of the boron atoms. This conclusion is substantiated by the observation that the fluoride binding constant of $[2]^+$ exceeds that of its neutral precursor by at least 4 orders of magnitude. A more general lesson that can be derived from this work is that chelate and Coulombic effects are additive and can be combined to boost the anion affinity of bidentate Lewis acids.

EXPERIMENTAL SECTION

General Considerations. Commercially available chemicals were purchased and used as provided (commercial sources: Aldrich for Mes_2BF , TMEDA, $[(\text{Me}_2\text{N})_3\text{S}][\text{Me}_3\text{SiF}_2]$, $[\text{nBu}_4\text{N}][\text{Ph}_3\text{SiF}_2]$, TMSCl, nBu_4NF , nBu_4NCl , nBu_4NBr , nBu_4NI , and nBu_4NN_3 ; TCI America for Ph_2S ; Alfa Aesar for BBr_3 and *n*-butyllithium (2.8 M in hexanes)). Diborane **1** was prepared by reaction of tetrakis(THF)lithium dimesityl-1,8-naphthalenediylborate^{7b,15} with 10-bromo-9-thia-10-boranthracene as previously described.^{8a} Solvents were dried by reflux under N_2 over drying agents and freshly distilled prior to use. The drying agents employed were CaH_2 for dichloromethane and Na/K for diethyl ether and THF. Air-sensitive compounds were handled under N_2 atmosphere using standard Schlenk and glovebox techniques. UV–vis spectra were recorded on an Ocean Optics USB4000 spectrometer with an Ocean Optics ISS light source. Elemental analyses were performed at Atlantic Microlab (Norcross, GA, USA). NMR spectra were recorded on Varian Unity Inova 400 FT NMR (399.59 MHz for ^1H , 376.03 MHz for ^{19}F , 128.19 MHz for ^{11}B , 100.45 MHz for ^{13}C) spectrometers at ambient temperature. Chemical shifts δ are given in ppm and are referenced against external $\text{BF}_3\cdot\text{Et}_2\text{O}$ (^{11}B and ^{19}F).

Crystallography. The crystallographic measurements were performed using a Bruker APEX-II CCD area detector diffractometer

(Mo $K\alpha$ radiation, $\lambda = 0.71069$ Å) for $[2]\text{OTf}$, $2-\mu_2\text{-F}$, and $2-\mu_2\text{-N}_3$. In each case, a specimen of suitable size and quality was selected and mounted onto a nylon loop. The structures were solved by direct methods, which successfully located most of the non-hydrogen atoms. Subsequent refinement on F^2 using the SHELXTL/PC package (version 5.1) allowed location of the remaining non-hydrogen atoms.

Synthesis of $[2]\text{OTf}$. Methyl triflate (0.1 mL, 0.89 mmol) was added to a solution of diborane **2** (0.2 g, 0.35 mmol) in dichloromethane (10 mL) at room temperature. The mixture was refluxed overnight and then cooled to room temperature. The solvent was removed under vacuum to yield a solid, which was washed with diethyl ether to afford $[2]\text{OTf}$ as a pale yellow product (0.21 g, yield 81%). Single crystals of $[2]\text{OTf}\cdot\text{CH}_2\text{Cl}_2$ were obtained by slow diffusion of diethyl ether into a dichloromethane solution of $[2]\text{OTf}$ at -25 °C. ^1H NMR (CDCl_3): δ 0.95 (s, 3H, Mes- CH_3), 1.39 (s, 3H, Mes- CH_3), 1.47 (s, 3H, Mes- CH_3), 1.82 (s, 3H, Mes- CH_3), 1.84 (s, 3H, Mes- CH_3), 2.23 (s, 3H, Mes- CH_3), 3.60 (s, 3H, S- CH_3), 5.71 (s, 1H, Mes-CH), 6.59 (s, 1H, Mes-CH), 6.60 (s, 1H, Mes-CH), 6.69 (s, 1H, Mes-CH), 7.39 (d, 1H, $^3J(\text{HH}) = 7.2$ Hz, nap-CH), 7.46 (t, 1H, $^3J(\text{HH}) = 7.2$ Hz, nap-CH), 7.52 (d, 1H, $^3J(\text{HH}) = 7.6$ Hz, nap-CH), 7.53–7.63 (m, 3H, nap-CH), 7.77 (t, 1H, $^3J(\text{HH}) = 8.0$ Hz, CH), 7.82 (t, 1H, $^3J(\text{HH}) = 7.6$ Hz, CH), 7.88–7.94 (m, 2H, CH), 8.04 (d, 1H, $^3J(\text{HH}) = 8.4$ Hz, CH), 8.13 (d, 1H, $^3J(\text{HH}) = 8.0$ Hz, CH), 8.18 (d, 1H, $^3J(\text{HH}) = 8.0$ Hz, CH), 8.23 (d, 1H, $^3J(\text{HH}) = 8.0$ Hz, CH). ^{13}C NMR (CDCl_3): δ 21.00 (Mes- CH_3), 21.11 (Mes- CH_3), 21.19 (Mes- CH_3), 22.11 (Mes- CH_3), 23.74 (Mes- CH_3), 23.89 (Mes- CH_3), 25.26 (S- CH_3), 124.39, 126.51, 126.87, 127.40, 128.20, 128.29, 128.96, 130.12, 130.85, 130.88, 131.70, 132.28, 132.48, 132.51, 132.99, 133.13, 133.40, 133.98, 134.22, 135.93, 137.71, 138.64, 139.18, 139.76, 140.44, 141.47, 142.80, 143.49, 145.42, 147.93. ^{11}B NMR (CDCl_3): not detected. Anal. Calcd for $\text{C}_{42}\text{H}_{39}\text{B}_2\text{F}_3\text{O}_3\text{S}_2\cdot\text{CH}_2\text{Cl}_2$: C 63.03; H 5.04. Found: C 65.74; H 5.28. (The sample used for EA was obtained by recrystallization from CH_2Cl_2 ; the EA results indicate $\sim 50\%$ loss of interstitial CH_2Cl_2 molecule. The calculated values for $\text{C}_{42}\text{H}_{39}\text{B}_2\text{F}_3\text{O}_3\text{S}_2\cdot 1/2(\text{CH}_2\text{Cl}_2)$ are C 65.70; H 5.19.)

Synthesis of $2-\mu_2\text{-F}$. To a solution of $[2]\text{OTf}$ (50 mg, 0.068 mmol) in CH_2Cl_2 (5 mL) at 25 °C was added a CH_2Cl_2 solution (5 mL) of $[(\text{Me}_2\text{N})_3\text{S}][\text{Me}_3\text{SiF}_2]$ (21 mg, 0.076 mmol). After 15 min, the solvent was evaporated and the residue was dissolved in a mixture of CH_2Cl_2 (2 mL) and diethyl ether (18 mL). The resulting solution was filtered and evaporated to dryness to afford $2-\mu_2\text{-F}$ as a colorless solid (35 mg, 85% yield). Large colorless monocrystals of $2-\mu_2\text{-F}$ could be obtained by slow evaporation of an acetone solution of $2-\mu_2\text{-F}$ at room temperature. ^1H NMR (CDCl_3): δ 0.86 (s, 3H, Mes- CH_3), 1.63 (s, 3H, Mes- CH_3), 1.79 (s, 3H, Mes- CH_3), 1.92 (d, 3H, $J(\text{H}-\text{F}) = 5.2$ Hz, Mes- CH_3), 2.07 (s, 3H, Mes- CH_3), 2.23 (s, 3H, Mes- CH_3), 3.28 (s, 3H, S- CH_3), 5.99 (s, 1H, Mes-CH), 6.37 (s, 1H, Mes-CH), 6.39 (s, 1H, Mes-CH), 6.62–6.66 (m, 2H, CH), 6.67 (s, 1H, Mes-CH), 6.78 (d, 1H, $^3J(\text{HH}) = 7.2$ Hz, CH), 7.00 (t, 1H, $^3J(\text{HH}) = 7.6$ Hz, CH), 7.12–7.25 (m, SH, CH), 7.35 (t, 1H, $^3J(\text{HH}) = 7.6$ Hz, CH), 7.49 (dd, 2H, $^3J(\text{HH}) = 6.8$ Hz, CH), 7.75 (d, 1H, $^3J(\text{HH}) = 8.0$ Hz, CH), 7.87 (d, 1H, $^3J(\text{HH}) = 8.0$ Hz, CH). ^{13}C NMR (CDCl_3): δ 20.74 (Mes- CH_3), 21.01 (Mes- CH_3), 22.89 (Mes- CH_3), 24.58 (Mes- CH_3), 25.16 (Mes- CH_3), 25.24 (Mes- CH_3), 39.23 (S- CH_3), 124.20, 125.12, 125.92, 126.47, 126.68, 127.17, 127.47, 127.70, 127.92, 127.95, 128.01, 128.22, 129.16, 123.00 (d, $J(\text{CF}) = 7.3$ Hz), 130.50 (d, $J(\text{CF}) = 7.1$ Hz), 132.24 (d, $J(\text{CF}) = 6.8$ Hz), 132.61 (d, $J(\text{CF}) = 2.7$ Hz), 134.97 (d, $J(\text{CF}) = 1.9$ Hz), 135.10, 140.37, 140.76 (d, $J(\text{CF}) = 6.2$ Hz), 140.98, 141.57, 141.73 (d, $J(\text{CF}) = 5.9$ Hz), 141.84 (d, $J(\text{CF}) = 6.1$ Hz), 142.90. ^{11}B NMR (CDCl_3): +0.4 (s), +4.4 (bs). ^{19}F NMR (CDCl_3): -174.4 (s). Anal. Calcd for $\text{C}_{41}\text{H}_{39}\text{B}_2\text{FS}$: C 80.47; H 6.50. Found: C 80.91; H 6.49.

Synthesis of $2-\mu_2\text{-N}_3$. To a solution of $[2]\text{OTf}$ (84 mg, 0.11 mmol) in CH_2Cl_2 (5 mL) at 25 °C was added a CH_2Cl_2 solution (5 mL) of nBu_4NN_3 (35 mg, 0.12 mmol). After 15 min, the solvent was evaporated and the residue was dissolved in a solvent mixture of CH_2Cl_2 (2 mL) and diethyl ether (18 mL). The resulting solution was filtered and evaporated to dryness to afford $2-\mu_2\text{-N}_3$ as a colorless solid (41 mg, 59% yield). Large colorless monocrystals of $2-\mu_2\text{-N}_3$ could be obtained by slow evaporation of an acetone/hexane mixture of $2-\mu_2\text{-N}_3$ at room temperature. ^1H NMR (CDCl_3): δ 1.25 (s, 3H, Mes- CH_3),

1.73 (s, 3H, Mes-CH₃), 1.81 (s, 3H, Mes-CH₃), 2.10 (s, 6H, Mes-CH₃), 2.23 (s, 3H, Mes-CH₃), 3.26 (s, 3H, S-CH₃), 6.15 (bs, 1H, Mes-CH), 6.34 (bs, 1H, Mes-CH), 6.38 (d, 2H, ³J(HH) = 8.0 Hz, CH), 6.73 (bs, 1H, Mes-CH), 6.86 (bs, 1H, Mes-CH), 6.78 (m, 2H, CH), 7.06 (t, 1H, ³J(HH) = 6.0 Hz, CH), 7.18–7.33 (m, 4H, CH), 7.40–7.48 (m, 3H, CH), 7.66 (d, 1H, ³J(HH) = 8.0 Hz, CH), 7.77 (d, 1H, ³J(HH) = 8.0 Hz, CH). ¹³C NMR (CDCl₃): 20.73 (Mes-CH₃), 23.87 (Mes-CH₃), 25.41 (Mes-CH₃), 26.08 (Mes-CH₃), 30.95 (Mes-CH₃), 41.16 (S-CH₃), 123.73, 123.83, 125.03, 125.18, 126.08, 126.15, 126.31, 126.37, 126.86, 127.83, 128.15, 129.07, 129.57, 130.06, 130.68, 131.50, 132.52, 132.87, 133.07, 133.57, 133.95, 139.74, 140.53, 142.75. ¹¹B NMR (CDCl₃): -4.6. Anal. Calcd for C₄₁H₃₉B₂N₃S: C 78.48; H 6.26. Found: C 78.36; H 6.37.

Anion (X⁻) Complexation in CHCl₃. A CHCl₃ solution of [2]⁺OTf (3 mL, c = 6.73 × 10⁻⁵ M for X⁻ = F⁻ and c = 9.5 × 10⁻⁵ M for X⁻ = N₃⁻) was placed in a cuvette and titrated with incremental amounts of the anion by addition of a CHCl₃ solution of [nBu₄N][Ph₃SiF₂] for X⁻ = F⁻ (7.2 mM) or nBu₄NN₃ for X⁻ = N₃⁻ (33.5 mM). For both experiments, the absorbance of the diborane was monitored at λ = 349 nm, showing stoichiometric complexation of the anion (ε = 10 040 for [2]⁺OTf, ε = 3270 for 2-μ₂-F, ε = 3100 for 2-μ₂-N₃).

NMR Study of the Reaction of Diborane 1 with [nBu₄N][Ph₃SiF₂] in CDCl₃. In a typical assay, a mixture of diborane 1 and [nBu₄N][Ph₃SiF₂] in CDCl₃ was placed in an NMR tube and analyzed by ¹H NMR and ¹⁹F NMR spectroscopy. Integration of the spectra was used to determine the respective concentration of the relevant species. Two data sets (labeled as experiments 1 and 2) are provided below, along with the derivation of the equation used to calculate K_{rel}(1) (F₀ is the initial concentration of Ph₃SiF₂⁻, and B₀ is the initial concentration of the diborane 1).

	1	+ Ph ₃ SiF	+ 2 × F ⁻	⇌	1F ⁻	+ Ph ₃ SiF ₂ ⁻
	B ₀ - x	F ₀ - y	F ₀ - x - y		x	y
experiment 1	5.1	51			51	100
experiment 2	70	100			100	25

$K_1 = \frac{[1F^-]}{([1]^*[F^-])} = \frac{x}{[(B_0 - x)(F_0 - x - y)]}$. $K_{Ph_3SiF_2^-} = \frac{[Ph_3SiF_2^-]}{([Ph_3SiF][F^-])} = \frac{y}{[(F_0 - y)(F_0 - x - y)]} \Rightarrow K_{rel}(1) = \frac{K_1}{K_{Ph_3SiF_2^-}} = \frac{[x(F_0 - y)]}{[y(B_0 - x)]} = 5.4 (\pm 1)$.

Electrochemistry. Electrochemical experiments were performed with an electrochemical analyzer from CH Instruments (model 610A) with a glassy carbon working electrode, a platinum auxiliary electrode, and a reference silver electrode. The reference electrode solution was built by immersing a silver wire in a Vycor-capped glass tube containing a THF solution of [nBu₄N][PF₆] (0.1 M) and AgNO₃ (0.005 M). All three electrodes were placed in a THF solution (3 mL) containing [nBu₄N][PF₆] (0.1 M) as supporting electrolyte and [2]⁺OTf (0.010 M). Ferrocene was used as an internal standard, and the potentials are reported relative to the E_{1/2} of the Fc⁺/Fc redox couple.

Computational Details. DFT calculations (full geometry optimization) were carried out with the Gaussian 03 program using the gradient-corrected Becke exchange functional (B3LYP) and the Lee–Yang–Parr correlation functional. Geometry optimization was carried out with the following mixed basis set: 6-31+G(d') for the boron, nitrogen, and fluorine atoms, 6-31+G(d) for the sulfur atom, and the 6-31G basis set was used for the other remaining carbon and hydrogen atoms. Frequency calculations for [2]⁺, 2-μ₂-F, and 2-μ₂-N₃ confirmed the absence of any imaginary frequencies. In the case of 2-F (τ = 101.3°), a weakly negative frequency associated with a methyl group rotation at the *para*-position of one of the mesityl groups was identified. All other structures with the τ angle constrained to specific values are not minima and were therefore not subjected to frequency calculations. DT-DFT calculation was carried out with the Gaussian 03 program using the B3LYP functional with the same basis sets as the DFT calculation. The transition state of the sulfonium unit inversion reaction was located with the synchronous transit-guided quasi-Newton

(STQN) method and further confirmed by the intrinsic reaction coordinate method (see Table S1 and Figure S1 in the Supporting Information).

■ ASSOCIATED CONTENT

Supporting Information

Cartesian coordinates of the optimized structures and X-ray data in CIF format. These materials are available free of charge via the Internet at <http://pubs.acs.org>.

■ AUTHOR INFORMATION

Corresponding Author

*E-mail: francois@tamu.edu.

Notes

The authors declare no competing financial interest.

■ ACKNOWLEDGMENTS

This work was supported by the National Science Foundation (CHE-0952912), the Welch Foundation (A-1423), and Texas A&M. We thank Ching-Wen Chiu for her original contribution to this project.

■ REFERENCES

- (a) Biallas, M. J.; Shriver, D. F. *J. Am. Chem. Soc.* **1966**, *88*, 375–376. (b) Katz, H. E. *Inclusion Compd.* **1991**, *4*, 391–405. (c) Schmidtchen, F. P.; Berger, M. *Chem. Rev.* **1997**, *97*, 1609–1646. (d) Gabbai, F. P. *Angew. Chem., Int. Ed.* **2003**, *42*, 2218–2221. (e) Melaïmi, M.; Gabbai, F. P. *Adv. Organomet. Chem.* **2005**, *53*, 61–99. (f) Wang, H.; Sole, S.; Gabbai, F. P. *ACS Symp. Ser.* **2006**, *917*, 208–220.
- (a) Hudnall, T. W.; Chiu, C.-W.; Gabbai, F. P. *Acc. Chem. Res.* **2009**, *42*, 388–397. (b) Wade, C. R.; Broomsgrove, A. E. J.; Aldridge, S.; Gabbai, F. P. *Chem. Rev.* **2010**, *110*, 3958–3984.
- (a) Williams, V. C.; Piers, W. E.; Clegg, W.; Elsegood, M. R. J.; Collins, S.; Marder, T. B. *J. Am. Chem. Soc.* **1999**, *121*, 3244–3245. (b) Piers, W. E.; Irvine, G. J.; Williams, V. C. *Eur. J. Inorg. Chem.* **2000**, 2131–2142. (c) Lewis, S. P.; Taylor, N. J.; Piers, W. E.; Collins, S. *J. Am. Chem. Soc.* **2003**, *125*, 14686–14687. (d) Zhao, H.; Gabbai, F. P. *Org. Lett.* **2011**, 1444–1446.
- (a) Jiang, C.; Blacque, O.; Berke, H. *Chem. Commun.* **2009**, 5518–5520. (b) Zhao, X.; Stephan, D. W. *Chem. Commun.* **2011**, *47*, 1833–1835.
- (a) Chiu, C.-W.; Gabbai, F. P. *J. Am. Chem. Soc.* **2006**, *128*, 14248–14249. (b) Hudnall, T. W.; Kim, Y.-M.; Bebbington, M. W. P.; Bourissou, D.; Gabbai, F. P. *J. Am. Chem. Soc.* **2008**, *130*, 10890–10891. (c) Kim, Y.; Hudnall, T. W.; Bouhadir, G.; Bourissou, D.; Gabbai, F. P. *Chem. Commun.* **2009**, 3729–3731. (d) Kim, Y.; Zhao, H.; Gabbai, F. P. *Angew. Chem., Int. Ed.* **2009**, *48*, 4957–4960. (e) Agou, T.; Sekine, M.; Kobayashi, J.; Kawashima, T. *Chem.—Eur. J.* **2009**, *15*, 5056–5062. (f) Wade, C. R.; Zhao, H.; Gabbai, F. P. *Chem. Commun.* **2010**, *46*, 6380–6381. (g) Broomsgrove, A. E. J.; Addy, D.; Di Paolo, A.; Morgan, I. R.; Bresner, C.; Chislett, V.; Fallis, I. A.; Thompson, A. L.; Vidovic, D.; Aldridge, S. *Inorg. Chem.* **2010**, *49*, 157–173. (h) Wade, C. R.; Gabbai, F. P. *Organometallics* **2011**, *30*, 4479–4481. (i) Zhao, H.; Gabbai, F. P. *Nat. Chem.* **2010**, *2*, 984–990. (j) Kim, Y.; Gabbai, F. P. *J. Am. Chem. Soc.* **2009**, *131*, 3363–3369.
- (a) Katz, H. E. *J. Org. Chem.* **1985**, *50*, 5027–5032. (b) Katz, H. E. *J. Am. Chem. Soc.* **1985**, *107*, 1420–1421. (c) Katz, H. E. *Organometallics* **1987**, *6*, 1134–1136.
- (a) Hoefelmeyer, J. D.; Gabbai, F. P. *J. Am. Chem. Soc.* **2000**, *122*, 9054–9055. (b) Hoefelmeyer, J. D.; Gabbai, F. P. *Organometallics* **2002**, *21*, 982–985. (c) Hoefelmeyer, J. D.; Schulte, M.; Tschinkl, M.; Gabbai, F. P. *Coord. Chem. Rev.* **2002**, *235*, 93–103. (d) Hoefelmeyer, J. D.; Solé, S.; Gabbai, F. P. *Dalton Trans.* **2004**, 1254–1258.

- (8) (a) Solé, S.; Gabbai, F. P. *Chem. Commun.* **2004**, 1284–1285.
(b) Melaimi, M.; Sole, S.; Chiu, C.-W.; Wang, H.; Gabbai, F. P. *Inorg. Chem.* **2006**, *45*, 8136–8143.
- (9) (a) Agou, T.; Kobayashi, J.; Kawashima, T. *Chem.—Eur. J.* **2007**, *13*, 8051–8060. (b) Matsumoto, T.; Wade, C. R.; Gabbai, F. P. *Organometallics* **2010**, *29*, 5490–5495. (c) Agou, T.; Kobayashi, J.; Kawashima, T. *Phosphorus, Sulfur Silicon Relat. Elem.* **2010**, *185*, 947–951. (d) Rohr, A. D.; Banaszak, H. M. M.; Kampf, J. W.; Ashe, A. J. *Organometallics* **2011**, *30*, 3698–3700.
- (10) (a) Agou, T.; Kobayashi, J.; Kawashima, T. *Inorg. Chem.* **2006**, *45*, 9137–9144. (b) Lee, M. H.; Agou, T.; Kobayashi, J.; Kawashima, T.; Gabbai, F. P. *Chem. Commun.* **2007**, 1133–1135. (c) Agou, T.; Kobayashi, J.; Kim, Y.; Gabbai, F. P.; Kawashima, T. *Chem. Lett.* **2007**, *36*, 976–977.
- (11) Yamaguchi, S.; Akiyama, S.; Tamao, K. *J. Am. Chem. Soc.* **2001**, *123*, 11372–11375.
- (12) Dorsey, C. L.; Jewula, P.; Hudnall, T. W.; Hoefelmeyer, J. D.; Taylor, T. J.; Honesty, N. R.; Chiu, C.-W.; Schulte, M.; Gabbai, F. P. *Dalton Trans.* **2008**, 4442–4450.
- (13) Bader, R. F. W. *Atoms in Molecules: A Quantum Theory*; Oxford University Press: UK, 1994.
- (14) Kim, Y.; Kim, M.; Gabbai, F. P. *Org. Lett.* **2010**, *12*, 600–602.
- (15) Schulte, M.; Gabbai, F. P. *Chem.—Eur. J.* **2002**, *8*, 3802–3807.